NASA / CR-2002-211745

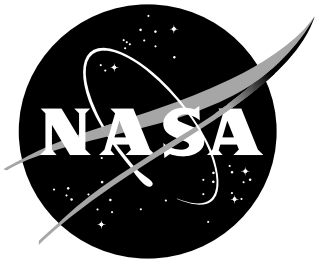


# Wake Vortex Algorithm Scoring Results

*R. E. Robins and D. P. Delisi*
*Northwest Research Associates, Inc.*
*Bellevue, Washington*

June 2002

# The NASA STI Program Office ... in Profile

Since its founding, NASA has been dedicated to the advancement of aeronautics and space science. The NASA Scientific and Technical Information (STI) Program Office plays a key part in helping NASA maintain this important role.

The NASA STI Program Office is operated by Langley Research Center, the lead center for NASA's scientific and technical information. The NASA STI Program Office provides access to the NASA STI Database, the largest collection of aeronautical and space science STI in the world. The Program Office is also NASA's institutional mechanism for disseminating the results of its research and development activities. These results are published by NASA in the NASA STI Report Series, which includes the following report types:

- TECHNICAL PUBLICATION. Reports of completed research or a major significant phase of research that present the results of NASA programs and include extensive data or theoretical analysis. Includes compilations of significant scientific and technical data and information deemed to be of continuing reference value. NASA counterpart of peer-reviewed formal professional papers, but having less stringent limitations on manuscript length and extent of graphic presentations.

- TECHNICAL MEMORANDUM. Scientific and technical findings that are preliminary or of specialized interest, e.g., quick release reports, working papers, and bibliographies that contain minimal annotation. Does not contain extensive analysis.

- CONTRACTOR REPORT. Scientific and technical findings by NASA-sponsored contractors and grantees.

- CONFERENCE PUBLICATION. Collected papers from scientific and technical conferences, symposia, seminars, or other meetings sponsored or co-sponsored by NASA.

- SPECIAL PUBLICATION. Scientific, technical, or historical information from NASA programs, projects, and missions, often concerned with subjects having substantial public interest.

- TECHNICAL TRANSLATION. English-language translations of foreign scientific and technical material pertinent to NASA's mission.

Specialized services that complement the STI Program Office's diverse offerings include creating custom thesauri, building customized databases, organizing and publishing research results ... even providing videos.

For more information about the NASA STI Program Office, see the following:

- Access the NASA STI Program Home Page at ***http://www.sti.nasa.gov***

- E-mail your question via the Internet to help@sti.nasa.gov

- Fax your question to the NASA STI Help Desk at (301) 621-0134

- Phone the NASA STI Help Desk at (301) 621-0390

- Write to:
  NASA STI Help Desk
  NASA Center for AeroSpace Information
  7121 Standard Drive
  Hanover, MD 21076-1320

NASA / CR-2002-211745

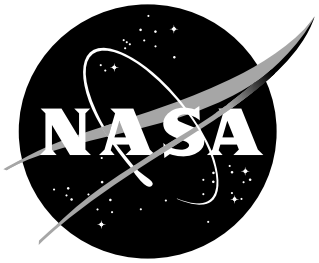


# Wake Vortex Algorithm Scoring Results

*R. E. Robins and D. P. Delisi*
*Northwest Research Associates, Inc.*
*Bellevue, Washington*

National Aeronautics and
Space Administration

Langley Research Center
Hampton, Virginia 23681-2199

Prepared for Langley Research Center
under Contract NAS1-99074

June 2002

Available from:

NASA Center for AeroSpace Information (CASI)
7121 Standard Drive
Hanover, MD 21076-1320
(301) 621-0390

National Technical Information Service (NTIS)
5285 Port Royal Road
Springfield, VA 22161-2171
(703) 605-6000

## Table of Contents

**Abstract** ..... ii

**1. Introduction** ..... 1

**2. Results of Algorithm Scoring** ..... 3

**3. Conclusions** ..... 9

**Acknowledgements** ..... 10

**References** ..... 10

**Tables** ..... 11

**Figures** ..... 14

**Appendix A. Description of the AVOSS Prediction Algorithm Data Base** ..... A-1

**Appendix B. Figures Showing EDR and TKE Model Predictions versus Observations for MEM Cases 1301 and 1245** ..... B-1

**Appendix C. Supplementary Performance Statistics for EDR Model** ..... C-1

**Abstract**

This report compares the performance of two models of trailing vortex evolution for which interaction with the ground is not a significant factor. One model uses eddy dissipation rate (EDR) and the other uses the kinetic energy of turbulence fluctuations (TKE) to represent the effect of turbulence. In other respects, the models are nearly identical. The models are evaluated by comparing their predictions of circulation decay, vertical descent, and lateral transport to observations for over four hundred cases from Memphis and Dallas / Fort Worth International Airports. These observations were obtained during deployments in support of NASA's Aircraft Vortex Spacing System (AVOSS). The results of the comparisons show that the EDR model usually performs slightly better than the TKE model.

# 1. Introduction

Within NASA's Terminal Area Productivity program, Langley Research Center (LaRC) has been developing a prototype Aircraft Vortex Spacing System (AVOSS). The purpose of AVOSS is to increase airport capacity by safely and reliably reducing the required minimum spacing between landing and/or departing aircraft by taking advantage of atmospheric conditions that may reduce the hazard to following aircraft from a preceding aircraft's trailing vorticity. A key component of AVOSS is a real-time algorithm for predicting the trajectories and circulation decay of the trailing vortices.

In order to satisfy the vortex prediction requirements of AVOSS, Northwest Research Associates (NWRA) has delivered the following prediction algorithms to the AVOSS team at NASA LaRC (the generic designation for these algorithms is APA, for AVOSS Prediction Algorithm):

Version 1 - initial algorithm; Greene's model (Greene, 1986) was enhanced to include vertical profiles of Brunt-Vaisala frequency, crosswind and turbulence kinetic energy (TKE), and three phases of ground effect; documented by Robins and Delisi (1997), and reported on by Robins et al. (1998).

Version 2 - improved edition of Version 1; ground effect portions of Version 1 were improved to prevent problems for vortex generation close to the ground. Results from this version were reported on by Robins and Delisi (1999).

Version 3.1 - out-of-ground-effect portion of Version 2 was replaced with a model allowing variable vortex separation and using eddy-dissipation rate (EDR) rather than TKE in the term describing circulation decay due to turbulence; a preliminary version of this model was described by Sarpkaya (1999), and the latest version was described by Sarpkaya et al. (2000) in a paper which included plotted and statistical comparisons between predictions and observations; the current version of AVOSS uses this version of APA.

Version 3.2 – version 3.1 was modified to include the effect of ground interaction on circulation decay; this modification is based on an analytic expression provided by Proctor et al. (2000) that is determined from results of TASS simulations.

Efforts are currently underway to explore how the Version 3.2 algorithm may be improved so that it is able to include effects due to shear and convection. A future Version 3.3 algorithm will include improvements coming out of these efforts.

In order to evaluate the performance of the prediction algorithms, a scoring procedure has been developed by NWRA (Robins and Delisi, 1999). The approach of this procedure is to run the algorithm being evaluated for most of the cases from previous deployments at Memphis (MEM) and Dallas/Fort Worth (DFW) airports, and to produce a database containing prediction-versus-observation statistics and other pertinent information for each case (a description of the database is provided in Appendix A). The vertical profiles of EDR and TKE for each case were generated by an algorithm developed at North Carolina State University (NCSU) with assistance from NWRA (Han et al., 2000). These profiles are designed to agree with measured values of TKE and EDR at an altitude of 40m. Measured TKE values are derived from 30 min. averages of 10 Hz data and the EDR values are from spectra of 30 min. periods of 10 Hz data. Note that for each case included in the database, the prediction-versus-observation statistics are computed only for the vortex (port or starboard) having the greatest number of good circulation observations.

The current status of algorithm scoring efforts is reported in the following section. Results from these efforts are summarized in Section 3. Supplementary statistics for the performance of Version 3.1 are presented in Appendix C.

## 2. Results of Algorithm Scoring

Prediction-versus-observation statistics from a large number of cases have been produced for Version 2 (TKE model) and Version 3.1 (EDR model) of APA. These results are presented in Tables 1, 1A, and 2 - 5, and are plotted in Figures 1, 1A, and 2-5. The tables are grouped in a "Tables" section and the figures in a "Figures" section. Each figure contains vertical bar charts of the values in the corresponding table.

In the TKE model, circulation decay due to turbulence is represented as

$$d\Gamma/dt = -k\Gamma q(z) / b_{0,}$$

where $\Gamma$ is circulation, t is time, q(z) is the turbulence velocity at altitude z, $b_0$ is $\pi/4$ times the aircraft wing span, and k is a constant. Note that q(z) is derived from boundary layer similarity theory (Han, et al., 2000), and at z = 40m is equal to the TKE obtained from a 30 min average of 10 Hz data measured at that altitude.

In the EDR model, circulation decay due to turbulence is obtained from the representation

$$\Gamma/\Gamma_0 = \exp(-CT/T^*),$$

where $\Gamma_0$ is the initial value of $\Gamma$, $T = t/T_0$, T* is non-dimensional demise time given in terms of the normalized dissipation rate, $\varepsilon^*$ (see Sarpkaya [2000] for the relation between T* and $\varepsilon^*$), and C is a constant. This equation is equivalent to $\frac{d\Gamma}{dT} = -\frac{c}{T^*}\Gamma$.

Using empirical methods described by Robins and Delisi (1999), the constant k in the TKE model was chosen to be 0.20, and the constant C in the EDR model was chosen to be 0.55.

It is important to note that predictions of circulation decay come from the expression $\Gamma=2\pi b_0 V$, where V, the vertical descent rate of the vortices is the primary variable solved for by either the TKE or the EDR model. The above expressions for $d\Gamma/dt$ and $\Gamma/\Gamma_0$ represent terms in the model equations and are not to be confused with similar quantities derived from solutions to the equations.

Shown in all tables are the median (Tables 1,2,3,4,5) or 90th percentile (Table 1A) values of four quantities: (i) RMS $\Delta\Gamma$ / $\Gamma_0$, (ii) Normalized $\Delta t$ to Leave the Corridor ($TTLC/T_0$), (iii) RMS $\Delta z$ / $b_0$, and (iv) RMS $\Delta y$ / $b_0$, where the corridor referred to in the second heading is the "floor two" AVOSS corridor defined by Hinton (1996). The first, third, and fourth quantities are RMS differences between predictions and observations, normalized by the appropriate initial value, either $\Gamma_0$ or $b_0$. These quantities are stored in AVOSS Prediction Algorithm Database fields 19, 17 and 21, respectively (see Appendix A). The second quantity is obtained from the database as abs(abs(field 12) - abs(field 13))/(field 33), where abs(field12) and abs(field 13) are the measured and predicted times, respectively, for a vortex to leave the AVOSS corridor, and field 33 is $T_0$. This quantity is evaluated only for those cases where both predicted and observed vortices actually exit the AVOSS corridor. Since there are always some cases for which either the predicted or the observed vortex does not exit the corridor, the number of cases indicated in the tables is always less for the second column than for the first, third and fourth columns. Note that for the purpose of scoring the algorithm, the initial altitude is taken to be the observed initial altitude for each case. This initial altitude is determined by backward extrapolation of the actual observed altitudes to a time of zero. In actual operation, AVOSS would use the glide slope height as the initial altitude of the vortices.

To clarify how the table values are derived, we note that, for each case, predicted and observed values are interpolated onto the same uniform time grid, after which the square of the difference between individual predicted and observed interpolated values is averaged over the duration of the case. The distribution of the square root of these

averages (the RMS values) is then analyzed, and median and 90th percentile values are entered into the tables. For a given case, only the RMS value for the vortex (port or starboard) with the most circulation observation values is used.

In all tables, the symbol $\Delta$ refers to the absolute difference between prediction and observation. t is time, which is normalized by $T_0$, the time it takes a vortex pair to descend a distance equal to the initial separation between the vortices, $b_0$; z is altitude and $\Gamma$ is circulation, $\Gamma_0$ being initial circulation. TKE and EDR refer to Version 2 and Version 3.1, respectively, of APA. MEM refers to the 1995 MEM deployment (August 6-29) and DFW refers to the 1997 DFW deployment (September 17 - October 3). The number of cases evaluated is indicated in the tables.

Table 1 and Figure 1 show median values for 211 MEM cases and 191 DFW cases. What the data show may be characterized as follows:

- EDR predictions for circulation are better than TKE predictions (15% better at MEM, 7% better at DFW).
- EDR and TKE predictions are comparable for time-to-leave-corridor and altitude.
- TKE predictions are very slightly better than EDR predictions for lateral position (1% better at MEM, 3% better at DFW).
- All predictions of time-to-leave-corridor, altitude, and lateral position are better for DFW than for MEM.

As discussed by Sarpkaya et al. (2000), the disparity between MEM and DFW most likely arises because the vortex observation times for the MEM cases are generally longer than for the DFW cases, with the result that the predictions have more time to deviate from the observations for MEM than for DFW. Figures B-1 and B-3 show EDR predictions versus observations for two MEM cases. TKE predictions for these cases

are shown in Figs. B-2 and B-4. These figures show results that are representative of the median values of RMS $\Delta\Gamma / \Gamma_0$ (Figs. B-1 and B-2) and TTLC/$T_0$ (Figs. B-3 and B-4).

Table 1A and Figure 1A show 90th percentile values for the same MEM and DFW cases as shown in Table 1 and Figure 1. Results from these values show no major qualitative differences from the results for the median values.

In order to determine whether aircraft size has any effect on the prediction capabilities of the models, we divided the MEM and DFW data sets into two categories: "big" aircraft (weighing more than 150,000 lbs.) and "medium" aircraft (weighing between 80,000 and 150,000 lbs.). Table 2 and Figure 2 show median values for big and medium aircraft from MEM. Similar results for DFW are shown in Table 3 and Figure 3. We chose the categories "big" and "medium" for the aircraft types observed at MEM and DFW since they did not fit neatly into the conventional categories of heavy and large. Note that all 211 MEM cases and 191 DFW cases are included in these categories. We do not compare MEM results with DFW results because most of the MEM cases were observed during early evening or night whereas most of the DFW cases were observed during the day.

At MEM there were 50 big and 161 medium aircraft cases, and at DFW there were 54 big and 137 medium aircraft cases. The number of cases for the various aircraft types at MEM and DFW are shown in the following table:

| | Big Aircraft | Medium Aircraft |
|---|---|---|
| MEM | 25 DC-10 | 86 B-727 |
| | 11 Airbus 300 | 57 DC-9 |
| | 9 Airbus 310 | 15 Airbus 320 |
| | 5 B-757 | 3 B-737 |

| | | |
|---|---|---|
| DFW | 36 B-757 | 107 MD-80 |
| | 10 B-767 | 24 B-727 |
| | 3 Airbus 300 | 5 B-737 |
| | 3 L-1011 | 1 Airbus 320 |
| | 1 B-747 | |
| | 1 MD-11 | |

With one exception, the results in Tables 2 and 3 and Figures 2 and 3 show that EDR-model versus TKE-model comparative performance was similar to what we observed in Tables 1 and 1A and Figures 1 and 1A. The exception is that the EDR lateral position results were better than TKE lateral position results for big aircraft at MEM and DFW.

When comparing results for big versus medium aircraft, it was quite striking to observe how much better the MEM predictions were for big aircraft than for medium aircraft (Figure 2). Both models did better for big aircraft than medium aircraft when predicting circulation decay and did significantly better for big aircraft when predicting time-to-leave-corridor, altitude, and lateral positions. The big-versus-medium difference was particularly significant for EDR and TKE predictions of time-to-leave-corridor. These results imply that most of the model-to-model differences shown in Table 1 and Figure 1 for MEM come from the medium and not the big aircraft.

For DFW, the same result (significantly better for big than medium aircraft) was seen for time-to-leave-corridor, but the reverse result (better for medium than big aircraft) was true for circulation decay and lateral position. For altitude, minor big-versus-medium EDR and TKE differences were seen. One strong conclusion from these results is that both MEM and DFW time-to-leave-corridor predictions by the EDR and TKE models were much better for big than for medium aircraft.

Possible explanations for the better results for larger aircraft are: (i) the median descent speed for the big aircraft is 1.82 m/sec and for the medium aircraft is 1.57 m/sec, thus the vortices from the big aircraft are stronger and tend to spend less time in the corridor than the vortices from the medium aircraft, which means that for the heavier aircraft there is less time for deviation between prediction and observation to occur; (ii) stronger vortices are easier for the lidar to track and hence the lidar observations are more accurate for stronger vortices; and (iii) stronger vortices may be less susceptible to non-modeled atmosphere effects such as convection currents.

Table 4 and Figure 4 show median values for high and low turbulence cases from MEM; similar results for DFW are shown in Table 5 and Figure 5. By high and low turbulence, we mean TKE (obtained from a 30 minute average of 10 Hz data collected at 40m altitude) greater than or less than 0.7 $m^2/sec^2$, respectively. There were 178 low and 33 high turbulence cases for MEM, and 119 low and 72 high turbulence cases for DFW. The intent of breaking up the cases into high and low turbulence groups was to determine whether ambient turbulence has any effect on the predictive capability of the models.

Figures 4 and 5 show that for time-to-leave-corridor and altitude, both models show better MEM and DFW results for low turbulence than for high turbulence. For circulation and lateral position, we see no clear trend.

For altitude and lateral position, EDR and TKE results are comparable, and with two exceptions, EDR results are better than TKE results for circulation and time-to-leave-corridor. The exceptions are MEM high-turbulence circulation results, in which case EDR and TKE results are equal, and MEM low-turbulence time-to-leave-corridor results, in which case TKE results are better than EDR results.

## 3. Conclusions

The following strong conclusions can be drawn from the scoring results:

(1) The EDR model frequently outperforms the TKE model, although the differences between the models are usually small. There are several cases where either the reverse is true or the models' performance is nearly equivalent.

(2) Time-to-leave-corridor is predicted much better for heavier aircraft by both the EDR and TKE models.

(3) Both models tend to do better when ambient turbulence intensity is low, although sometimes the differences between high and low turbulence results are small.

## Acknowledgements

We gratefully acknowledge the support and encouragement of D. A. Hinton and F. H. Proctor of NASA's Langley Research Center.

## References

Greene, G. C. (1986), "An Approximate Model of Vortex Decay in the Atmosphere," *Journal of Aircraft*, Vol. 23, No. 7, pp. 566-573.

Han, J., Shen, S., Arya, S.P., and Lin, Y.-L. (2000), "An Estimation of Turbulent Kinetic Energy and Energy Dissipation Rate Based on Atmospheric Boundary Layer Similarity Theory," NASA Contract Report CR-2000-210298.

Hinton, D. A. (1996), "An Aircraft Vortex Spacing System (AVOSS) for Dynamical Wake Vortex Spacing Criteria," NATO-AGARD-CP-584, pp. 5.1-5.9.

Proctor, Fred H., David W. Hamilton, and Jongil Han (2000), "Wake Vortex Transport and Decay in Ground Effect: Vortex Linking with the Ground," AIAA Paper 2000-0757, January.

Robins, R. E., and Delisi, D. P. (1997), "Formulation and Assessment of the NWRA AVOSS Wake Predictor Algorithm, Version 1," Northwest Research Associates, Inc., December.

Robins, R. E., and Delisi, D. P. (1999), "Further Development of a Wake Vortex Predictor Algorithm and Comparisons to Data," AIAA Paper 99-0757, January.

Robins, R. E., Delisi, D. P., and Greene, G. C. (1998), "Development and Validation of a Wake Vortex Predictor Algorithm," AIAA Paper 98-0665, January.

Sarpkaya, T. (1999), "New Model for Vortex Decay in the Atmosphere," *Journal of Aircraft*, Vol. 37, No. 1, pp. 53-61.

Sarpkaya, T., Robins, R.E, Delisi, D.P. (2000), "Wake-Vortex Eddy-Dissipation Model Predictions Compared with Observations," AIAA Paper 2000-0625, January.

Table 1. Median Values for Indicated Measures of Differences between Predictions and Observations (Number of Cases is Shown in Parentheses)

| Model / Site | RMS $\Delta\Gamma / \Gamma_0$ | Normalized $\Delta t$ to Leave Corridor | RMS $\Delta z / b_0$ | RMS $\Delta y / b_0$ |
|---|---|---|---|---|
| EDR / MEM | 0.145 (211) | 0.119 (187) | 0.415 (211) | 0.788 (211) |
| TKE / MEM | 0.171 (211) | 0.112 (186) | 0.431 (211) | 0.780 (211) |
| EDR / DFW | 0.156 (191) | 0.087 (180) | 0.236 (191) | 0.565 (191) |
| TKE / DFW | 0.168 (191) | 0.095 (180) | 0.226 (191) | 0.548 (191) |

Table 1A. 90th Percentile Values for Indicated Measures of Differences between Predictions and Observations (Number of Cases is Shown in Parentheses)

| Model / Site | RMS $\Delta\Gamma / \Gamma_0$ | Normalized $\Delta t$ to Leave Corridor | RMS $\Delta z / b_0$ | RMS $\Delta y / b_0$ |
|---|---|---|---|---|
| EDR / MEM | 0.272 (211) | 0.573 (187) | 0.931 (211) | 2.300 (211) |
| TKE / MEM | 0.316 (211) | 0.611 (186) | 0.923 (211) | 2.214 (211) |
| EDR / DFW | 0.248 (191) | 0.279 (180) | 0.500 (191) | 1.752 (191) |
| TKE / DFW | 0.271 (191) | 0.286 (180) | 0.487 (191) | 1.786 (191) |

Table 2. Median Values for Indicated Measures of Differences between Predictions and Observations (Number of Cases is Shown in Parentheses)

| Model / Subgroup | RMS $\Delta\Gamma / \Gamma_0$ | Normalized $\Delta t$ to Leave Corridor | RMS $\Delta z / b_0$ | RMS $\Delta y / b_0$ |
|---|---|---|---|---|
| EDR / MEM_Big | 0.128 (50) | 0.078 (43) | 0.336 (50) | 0.527 (50) |
| TKE / MEM_Big | 0.148 (50) | 0.071 (42) | 0.362 (50) | 0.669 (50) |
| EDR / MEM_Med | 0.149 (161) | 0.126 (144) | 0.459 (161) | 0.831 (161) |
| TKE / MEM_Med | 0.190 (161) | 0.132 (144) | 0.483 (161) | 0.820 (161) |

Table 3. Median Values for Indicated Measures of Differences between Predictions and Observations (Number of Cases is Shown in Parentheses)

| Model / Subgroup | RMS $\Delta\Gamma / \Gamma_0$ | Normalized $\Delta t$ to Leave Corridor | RMS $\Delta z / b_0$ | RMS $\Delta y / b_0$ |
|---|---|---|---|---|
| EDR / DFW_Big | 0.168 (54) | 0.060 (50) | 0.239 (54) | 0.655 (54) |
| TKE / DFW_Big | 0.183 (54) | 0.061 (50) | 0.217 (54) | 0.701 (54) |
| EDR / DFW_Med | 0.153 (137) | 0.101 (130) | 0.233 (137) | 0.531 (137) |
| TKE / DFW_Med | 0.163 (137) | 0.114 (130) | 0.232 (137) | 0.503 (137) |

Table 4. Median Values for Indicated Measures of Differences between Predictions and Observations (Number of Cases is Shown in Parentheses)

| Model / Subgroup | RMS $\Delta\Gamma / \Gamma_0$ | Normalized $\Delta t$ to Leave Corridor | RMS $\Delta z / b_0$ | RMS $\Delta y / b_0$ |
|---|---|---|---|---|
| EDR / MEM_HiTKE | 0.160 (33) | 0.143 (28) | 0.466 (33) | 0.734 (33) |
| TKE / MEM_HiTKE | 0.155 (33) | 0.211 (28) | 0.469 (33) | 0.766 (33) |
| EDR / MEM_LoTKE | 0.143 (178) | 0.115 (159) | 0.407 (178) | 0.790 (178) |
| TKE / MEM_LoTKE | 0.181 (178) | 0.095 (158) | 0.417 (178) | 0.785 (178) |

Table 5. Median Values for Indicated Measures of Differences between Predictions and Observations (Number of Cases is Shown in Parentheses)

| Model / Subgroup | RMS $\Delta\Gamma / \Gamma_0$ | Normalized $\Delta t$ to Leave Corridor | RMS $\Delta z / b_0$ | RMS $\Delta y / b_0$ |
|---|---|---|---|---|
| EDR / DFW_HiTKE | 0.154 (72) | 0.096 (65) | 0.241 (72) | 0.545 (72) |
| TKE / DFW_HiTKE | 0.160 (72) | 0.127 (65) | 0.251 (72) | 0.515 (72) |
| EDR / DFW_LoTKE | 0.156 (119) | 0.079 (115) | 0.228 (119) | 0.569 (119) |
| TKE / DFW_LoTKE | 0.184 (119) | 0.087 (115) | 0.220 (119) | 0.566 (119) |

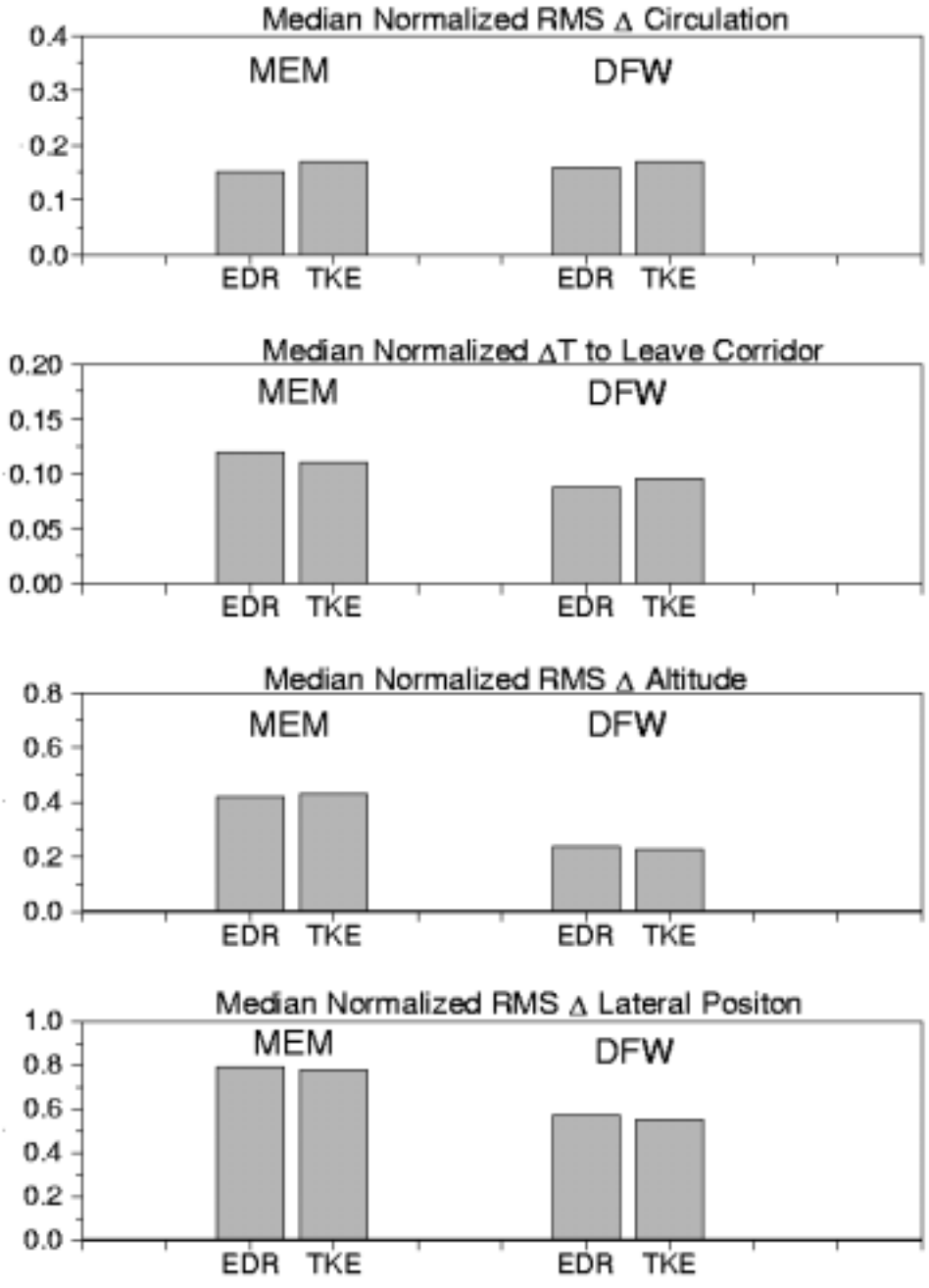


Figure 1. Median, normalized predictions versus observations for MEM and DFW

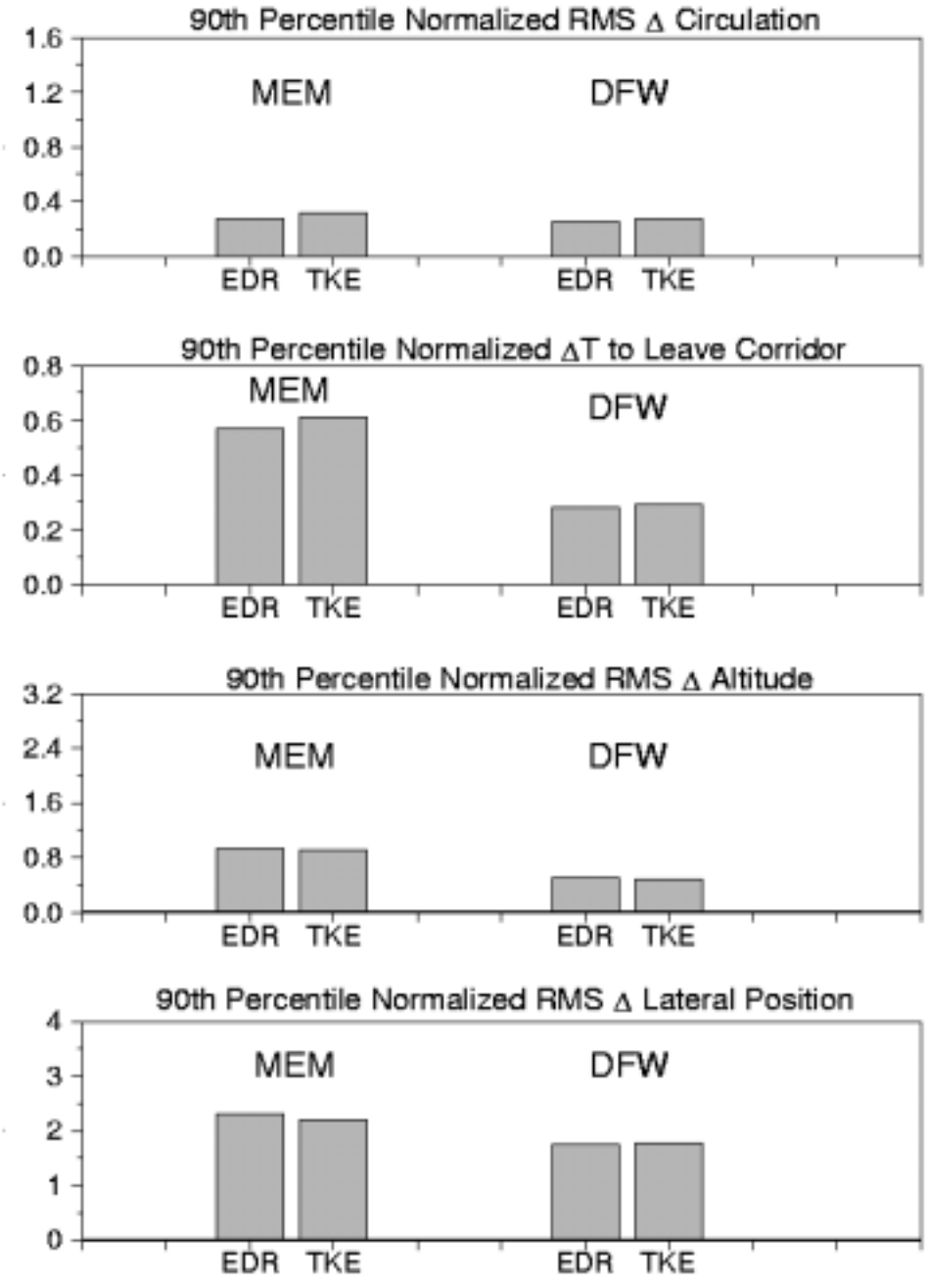


Figure 1A. 90th percentile, normalized predictions versus observations for MEM and DFW

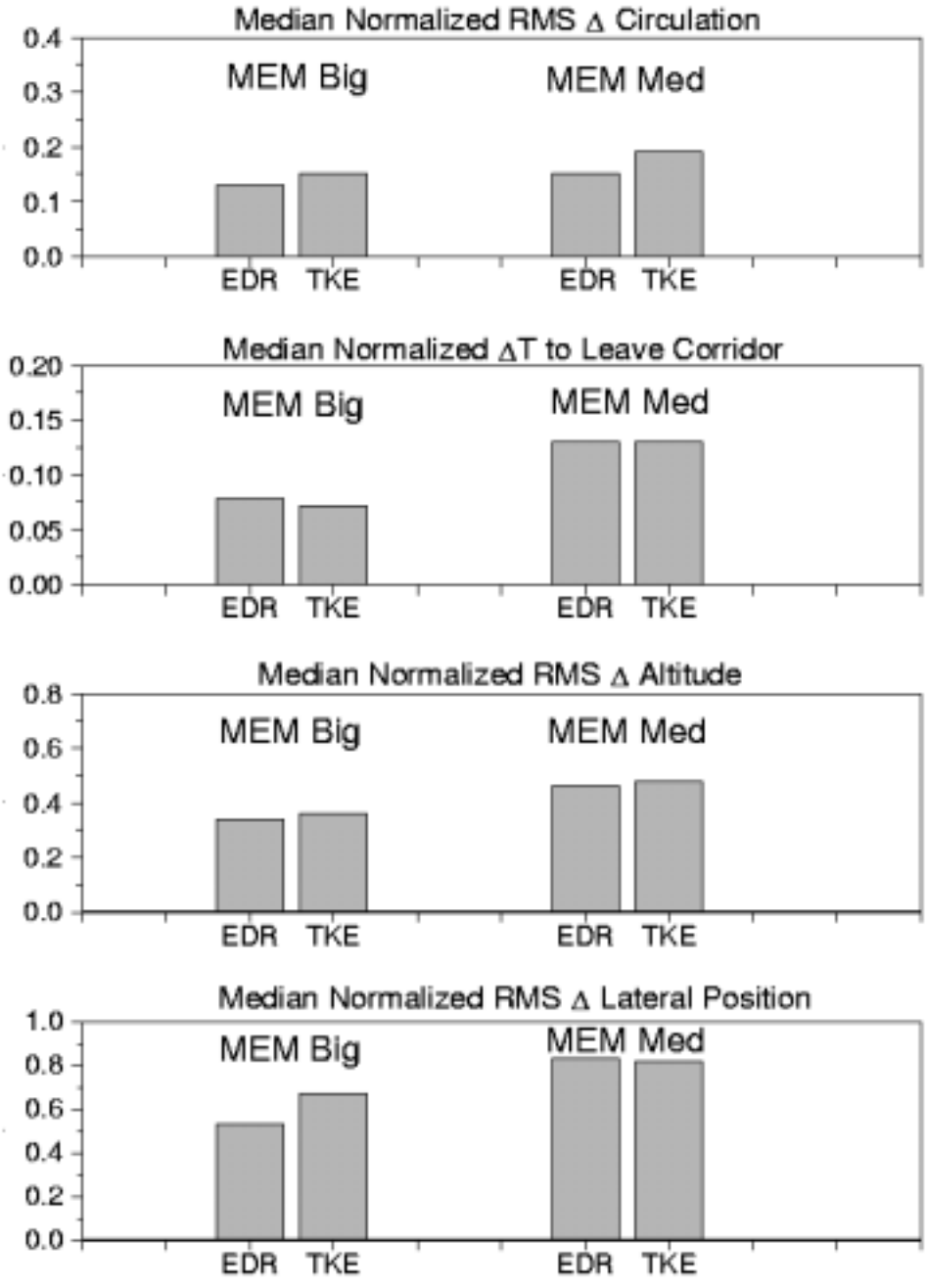


Figure 2. Median, normalized predictions versus observations for MEM Big and MEM Medium Aircraft

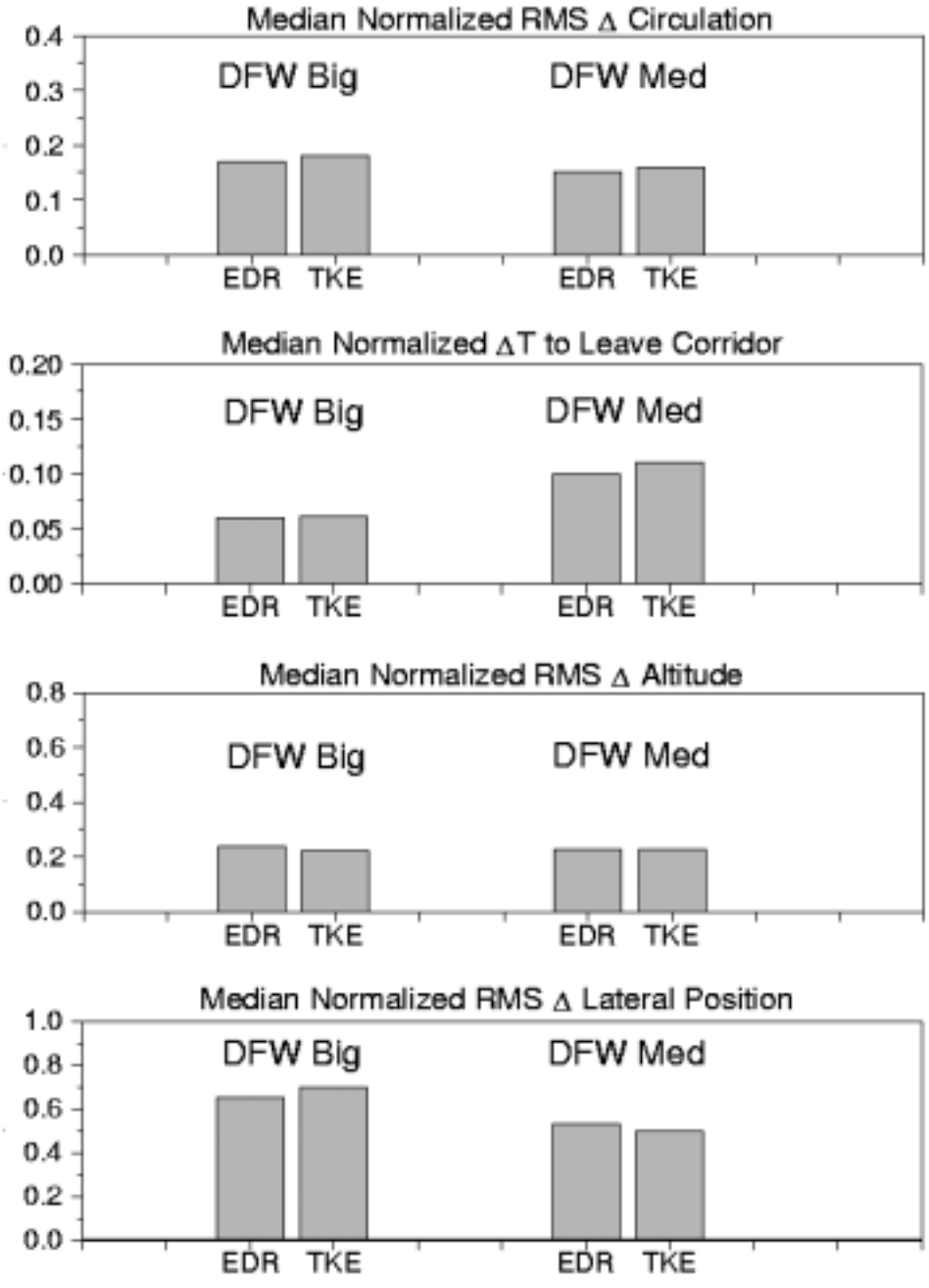


Figure 3. Median, normalized predictions versus observations for DFW Big and DFW Medium Aircraft

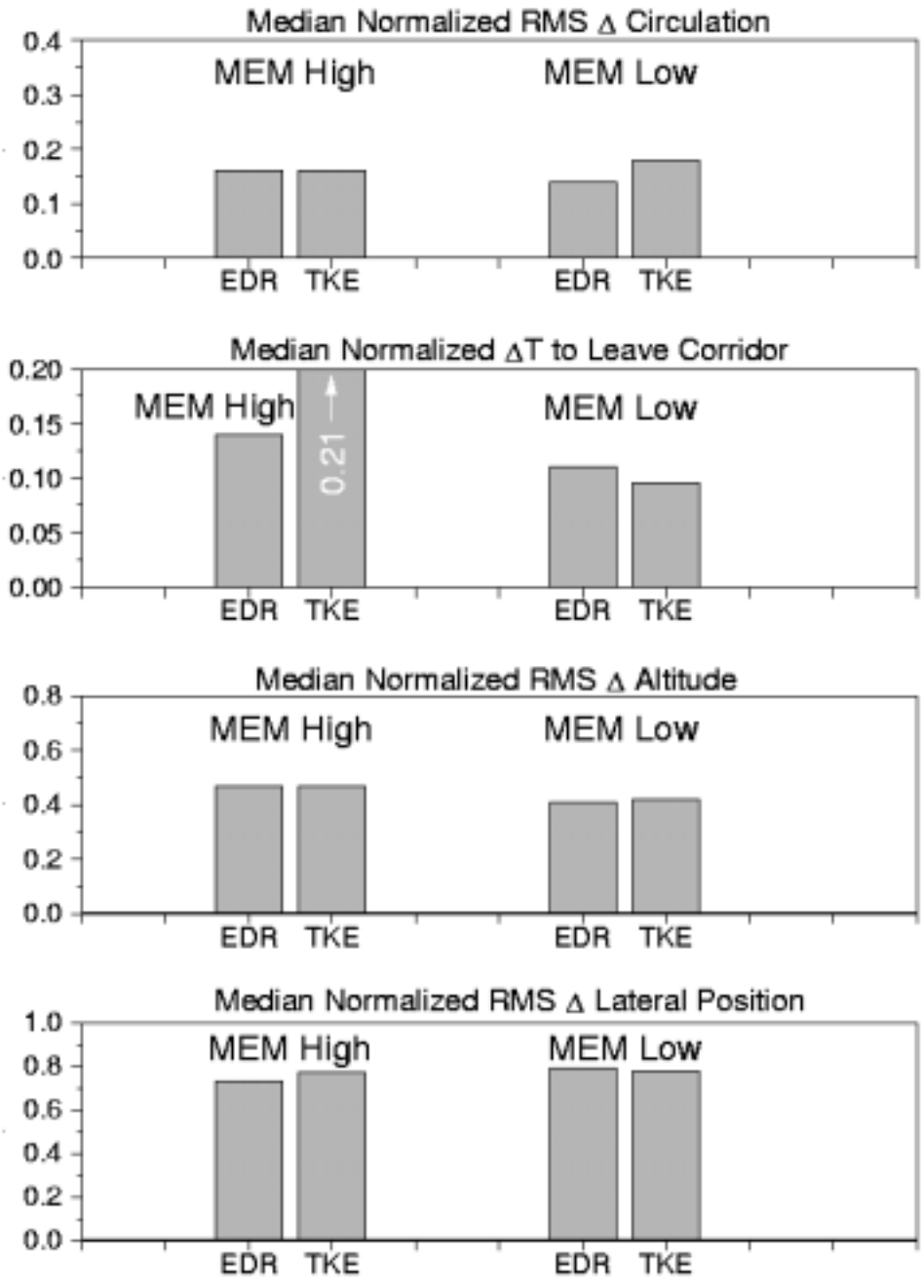


Figure 4. Median, normalized predictions versus observations for MEM High and MEM Low TKE Cases

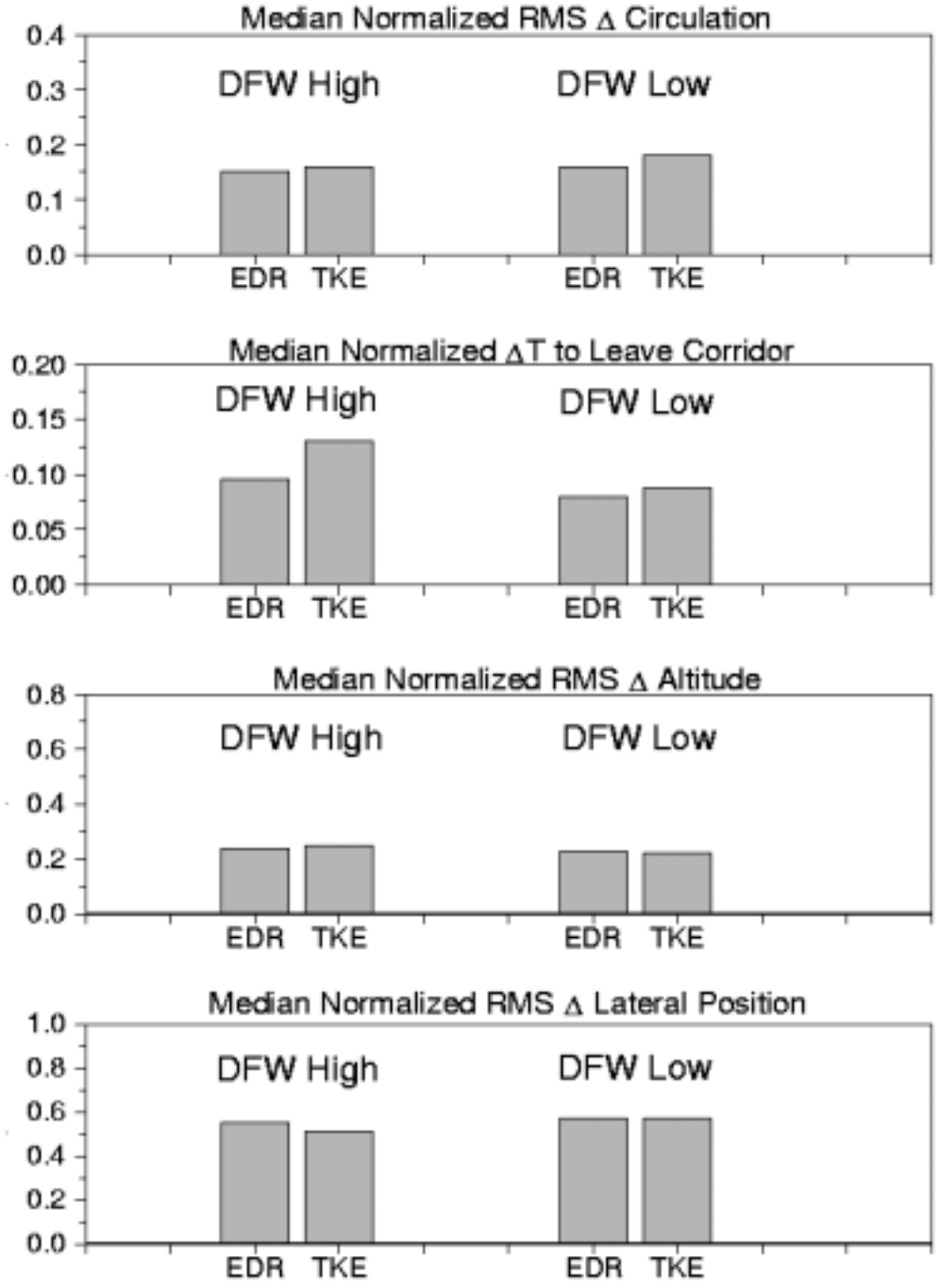


Figure 5. Median, normalized predictions versus observations for DFW High and DFW Low TKE Cases

## Appendix A. Description of the AVOSS Prediction Algorithm Data Base

The parameters in the database are grouped in five sections, each of which contains a collection of data fields that are related. Descriptions of the fields are as follows.

### Identification Information:

| Column | Acronym | Description |
|---|---|---|
| 1 | LOC | Location where data was acquired (e.g., MEM) |
| 2 | CASE | Number identifying the case (e.g., 1252) |
| 3 | STPO | Vortex identifier (STAR or PORT) |
| 4 | DATE | Date on which data acquisition was begun (e.g., 081695) |
| 5 | TIME | Time when data acquisition was begun (e.g., 025724) |
| 6 | SITE | Identifier for specific site where data was acquired |
| 7 | KIND | Kind of case (OGE, NGE, or IGE) |
| 8 | CORR | Corridor identifier |
| 9 | AIRC | Aircraft designation (e.g., B727) |
| 10 | MOD | Aircraft model (e.g., 200) |
| 11 | DUR | Duration of measured data (sec) |

### Primary Algorithm Evaluation Data:

| Column | Acronym | Description |
|---|---|---|
| 12 | OUTM | ABS(OUTM) is measured time for vortex to leave AVOSS corridor (sec) (OUTM < 0 for exit through corridor side) |
| 13 | OUTP | ABS(OUTP) is predicted time for vortex to leave AVOSS corridor (sec) (OUTP < 0) for exit through corridor side) |
| 14 | DTM1 | Measured time for circulation to drop below 150 m*m/sec (sec) |
| 15 | DTP1 | Predicted time for circulation to drop below 150 m*m/sec (sec) |
| 16 | ZRMS | RMS difference between measured and predicted vortex altitudes over entire run starting at t = 0 sec (m) |
| 17 | ZRMN | Normalized ZRMS, = ZRMS/BZ |
| 18 | GRMS | RMS difference between measured and predicted vortex circulations over entire run starting at t = 0 sec (m*m/sec) |
| 19 | GRMN | Normalized GRMS, = GRMS/GAMZ |
| 20 | YRMS | RMS difference between measured and predicted vortex lateral positions over time of entire run starting at t = 0 sec (m) |
| 21 | YRMN | Normalized YRMS, = YRMS/BZ |
| 22 | ZMXN | Maximum deviation between measured and predicted vortex altitudes, normalized by ZRMS |
| 23 | GMXN | Maximum deviation between measured and predicted vortex circulations, normalized by GRMS |
| 24 | YMXN | Maximum deviation between measured and predicted vortex lateral positions, normalized by YRMS |

**Acquisition Information:**

| Column | Acronym | Description |
|---|---|---|
| 25 | SPAN | Wingspan of aircraft (m) |
| 26 | WRPT | Reported landing weight of aircraft (kg), when available |
| 27 | WEST | Estimated landing weight of aircraft (kg), when WRPT is not available |
| 28 | UZ | Reported approach speed of aircraft (m/s) |
| 29 | RHOZ | Air density used to obtain GAMZ (kg/m^3) |
| 30 | GAMZ | Initial vortex circulation (m*m/sec), = WXXX/(BZ*UZ*RHOZ) where WXXX is either WRPT or WEST (see above) |
| 31 | BZ | Initial vortex separation (m), = (PI/4)*SPAN |
| 32 | VZ | Theoretical vortex descent rate (m/sec), = GAMZ/(2*PI*BZ) |
| 33 | TZ | Time for vortices to drop a distance of BZ (sec), TZ = BZ/VZ |
| 34 | ZZ | Initial altitude of vortex (m), based on backward extrapolation of altitude versus time data or subjectively chosen |
| 35 | ZZC | Either 'E', 'S', or 'F', depending whether ZZ is from backward extrapolation, subjectively chosen, or from first data point |
| 36 | YZ | Initial lateral offset of vortex from runway center (m), based on an average of the first few data points or subjectively chosen |
| 37 | YZC | Either 'E', 'S', or 'F', depending whether YZ is from backward extrapolation, subjectively chosen, or from first data point |

**Environmental Data:**

| Column | Acronym | Description |
|---|---|---|
| 38 | TKE5 | Observed turbulence kinetic energy (m*m/sec*sec) (5 min avg of 10 Hz data collected at a height of 40m) |
| 39 | QT | RMS turbulence velocity (m/sec), = SQRT(2*TKE) |
| 40 | QN | Normalized QT, = QT / VZ |
| 41 | TKE30 | Observed turbulence kinetic energy (m*m/sec*sec) (30 min avg of 10 Hz data collected at a height of 40m) |
| 42 | EDR | Eddy dissipation rate (m*m/sec^3) (from spectra of 10 Hz velocity data collected at an altitude of 40m) |
| 43 | EDRZ | NCSU modeled EDR at initial vortex altitude (m*m/sec^3) |
| 44 | EAV | Average eddy dissipation rate over vortex altitude range (m*m/sec^3) |
| 45 | EAVN | Normalized EAV, = (EAV*BZ)^(1/3) / VZ |
| 46 | TMOD | Value of normalized (by TZ) time corresponding to EAVN, according to Sarpkaya's model |
| 47 | NZ | BV frequency at initial vortex altitude (sec^-1) |
| 48 | NAV | Average BV frequency over vortex altitude range (sec^-1) |
| 49 | NN | Normalized NAV, = NAV * BZ / VZ |
| 50 | DCDZ | Temperature gradient over vortex altitude range (degC/m) |
| 51 | FRZ | Froude number (Fr) at initial vortex altitude |
| 52 | FRAV | Average Fr over vortex altitude range |

| | | |
|---|---|---|
| 53 | VZZ | Crosswind at initial vortex altitude (m/sec) |
| 54 | VMAX | Max crosswind over vortex altitude range (m/sec) |
| 55 | ZVMX | Altitude at which VMAX occurs (m) |
| 56 | VMIN | Min crosswind over vortex altitude range (m/sec) |
| 57 | ZVMN | Altitude at which VMIN occurs (m) |
| 58 | VAV | Average crosswind over vortex altitude range (m/sec) |
| 59 | GVMX | Max crosswind vertical shear over vortex altitude range (m/sec) |
| 60 | ZGVX | Altitude at which GVMX occurs (m) |
| 61 | GVMN | Min crosswind vertical shear over vortex altitude range (m/sec) |
| 62 | ZGVN | Altitude at which GVMN occurs (m) |
| 63 | RIMN | Min Richardson number (Ri) |
| 64 | ZRIN | Altitude at which RIMN occurs (m) |
| 65 | RIAV | Average Ri over vortex altitude range |
| 66 | GGVX | Max shear gradient (sec^-1) |
| 67 | ZGGX | Altitude at which GGZX occurs (m) |
| 68 | GGVN | Min shear gradient (sec^-1) |
| 69 | ZGGN | Altitude at which GGZN occurs (m) |

**Supplementary Algorithm Evaluation Data:**

| Column | Acronym | Description |
|---|---|---|
| 70 | DTM2 | Measured time for circulation to drop below 75 m*m/sec (sec) |
| 71 | DTP2 | Predicted time for circulation to drop below 75 m*m/sec (sec) |
| 72 | ZR30 | RMS difference between measured and predicted vortex altitudes over 0 to 30 sec (m) |
| 73 | GR30 | RMS difference between measured and predicted vortex circulations over 0 to 30 sec (m*m/sec) |
| 74 | YR30 | RMS difference between measured and predicted vortex lateral positions over 0 to 30 sec (m) |
| 75 | ZX30 | Maximum deviation between measured and predicted vortex altitudes over 0 to 30 sec normalized by ZR30 |
| 76 | GX30 | Maximum deviation between measured and predicted vortex circulations over 0 to 30 sec normalized by GR30 |
| 77 | YX30 | Maximum deviation between measured and predicted vortex lateral positions over 0 to 30 sec normalized by YR30 |
| 78 | ZR60 | RMS difference between measured and predicted vortex altitudes over 30 to 60 sec (m) |
| 79 | GR60 | RMS difference between measured and predicted vortex circulations over 30 to 60 sec (m*m/sec) |
| 80 | YR60 | RMS difference between measured and predicted vortex lateral positions over 30 to 60 sec (m) |
| 81 | ZX60 | Maximum deviation between measured and predicted vortex altitudes over 30 to 60 sec normalized by ZR60 |
| 82 | GX60 | Maximum deviation between measured and predicted vortex circulations over 30 to 60 sec normalized by GR60 |
| 83 | YX60 | Maximum deviation between measured and predicted vortex lateral positions over 30 to 60 sec normalized by YR60 |

| | | |
|---|---|---|
| 84 | ZR90 | RMS difference between measured and predicted vortex altitudes over 60 to 90 sec (m) |
| 85 | GR90 | RMS difference between measured and predicted vortex circulations over 60 to 90 sec (m*m/sec) |
| 86 | YR90 | RMS difference between measured and predicted vortex lateral positions over 60 to 90 sec (m) |
| 87 | ZX90 | Maximum deviation between measured and predicted vortex altitudes over 60 to 90 sec normalized by ZR90 |
| 88 | GX90 | Maximum deviation between measured and predicted vortex circulations over 60 to 90 sec normalized by GR90 |
| 89 | YX90 | Maximum deviation between measured and predicted vortex lateral positions over 60 to 90 sec normalized by YR90 |
| 90 | ZR120 | RMS difference between measured and predicted vortex altitudes over 90 to 120 sec (m) |
| 91 | GR120 | RMS difference between measured and predicted vortex circulations over 90 to 120 sec (m*m/sec) |
| 92 | YR120 | RMS difference between measured and predicted vortex lateral positions over 90 to 120 sec (m) |
| 93 | ZX120 | Maximum deviation between measured and predicted vortex altitudes over 90 to 120 sec normalized by ZR120 |
| 94 | GX120 | Maximum deviation between measured and predicted vortex circulations over 90 to 120 sec normalized by GR120 |
| 95 | YX120 | Maximum deviation between measured and predicted vortex lateral positions over 90 to 120 sec normalized by YR120 |

## Appendix B. Figures Showing EDR, and TKE Model Predictions versus Observations for MEM Cases 1301 and 1245

In this Appendix, we show plots that visualize the difference between results for the EDR and TKE models for cases that are representative of median values for $\Delta\Gamma/\Gamma_0$ and $TTLC/T_0$. In Figure B-1, we show results from an application of the EDR model for MEM case 1301, a case which occurred at the MEM Armory site. At the top of the figure is the case identifier (MEM1301), the date and universal time of the case, and the generating aircraft. On all plots the circles and ×'s are MIT/LL lidar observations of the port and starboard vortices, respectively.

The upper left plot shows observations and predictions for the vertical descent of the vortices; vortex altitude is plotted versus time. The heavy solid line shows the model prediction, and the thinner solid line emanating from the starting altitude represents descent at a constant speed, $V_0$, equal to $\Gamma_0 / 2\pi b_0$, where $\Gamma_0$ is the initial circulation and $b_0$ is the initial separation of the vortices ($\Gamma_0 = W/\rho U b_0$, where W is aircraft weight, $\rho$ is air density = 1.2 $kg/m^3$, and U is the aircraft speed). The horizontal thinner solid lines denote the upper and lower corridor floors of the safety corridor defined by Hinton (1996).

The lower left plot shows observations and predictions of circulation decay; circulation is plotted versus time. The observation data points are averages from three to ten meters of the circulation measured at radius intervals of one meter. Predictions for the port and starboard vortex are denoted by a solid heavy line. The long dashed line represents normalized circulation decay, $(1 / \Gamma_0)\, d\Gamma/dT$, at the rate $1 - T/8$, where T is time normalized by $b_0 / V_0$, and the short dashed line indicates the initial circulation level.

The lower right plot shows observations and predictions of the vortices' lateral motion, plotted versus time (note that time increases from the top to the bottom of the vertical axis). The heavy solid lines denote the predictions, and the vertical dashed line marks the center of the runway on which the aircraft was landing. The solid vertical line at the far right of the plot denotes the starboard edge of the AVOSS corridor, and the port edge of the AVOSS corridor is off the plot.

The upper right plot in Figure B-1 shows a plan view of the vortex motion. For both observations (symbols) and predictions (heavy solid lines), altitude is plotted versus lateral position. The vertical dashed line again marks the runway centerline, and the horizontal solid lines define the vertical extent of the AVOSS corridor, where the topmost line is at the altitude of the glide slope and the lower lines denote the upper and lower corridor floors. The solid vertical line at the far right of the plot denotes the starboard edge of the AVOSS corridor, and the port edge of the AVOSS corridor is off the plot. The vertical dotted line is midway between the vortices' initial lateral positions, and is used as the origin for plots of environmental profiles: a long dashed line for potential temperature and a thin solid line for cross wind. Five meters in lateral position represents one degree Kelvin of potential temperature, and one meter per second of cross wind. The vertical dotted line denotes the potential temperature at the ground and zero

cross-wind.

In Figure B-2, we show results from an application of the TKE model for MEM case 1301, the same case as shown in Figure B-1. The format for this figure is the same as for Figure B-1. The circulation decay results for these examples are typical of the median $\Delta\Gamma/\Gamma_0$ for all cases, as may be inferred from the following table;

| Figure | Case | Model | $\Delta\Gamma/\Gamma_0$ | Median $\Delta\Gamma/\Gamma_0$ |
|---|---|---|---|---|
| B-1 | 1301 | EDR | 0.159 | 0.145 |
| B-2 | 1301 | TKE | 0.148 | 0.171 |

The figures show that initially the rate of circulation decay is greater for the EDR model than for the TKE model.

In Figure B-3 and B-4, we show results from the EDR and TKE models for MEM case 1245. The formats for these figures are the same as for the previous figures. The normalized $\Delta t$ to leave corridor ($TTLC/T_0$) results for these examples are typical of the median $TTLC/T_0$ for all cases, as may be inferred from the following table:

| Figure | Case | Model | $TTLC/T_0$ | Median $TTLC/T_0$ |
|---|---|---|---|---|
| B-3 | 1245 | EDR | 0.095 | 0.119 |
| B-4 | 1245 | TKE | 0.112 | 0.112 |

The figures show that the descent of the vortices through the corridor is nearly identical for the two models.

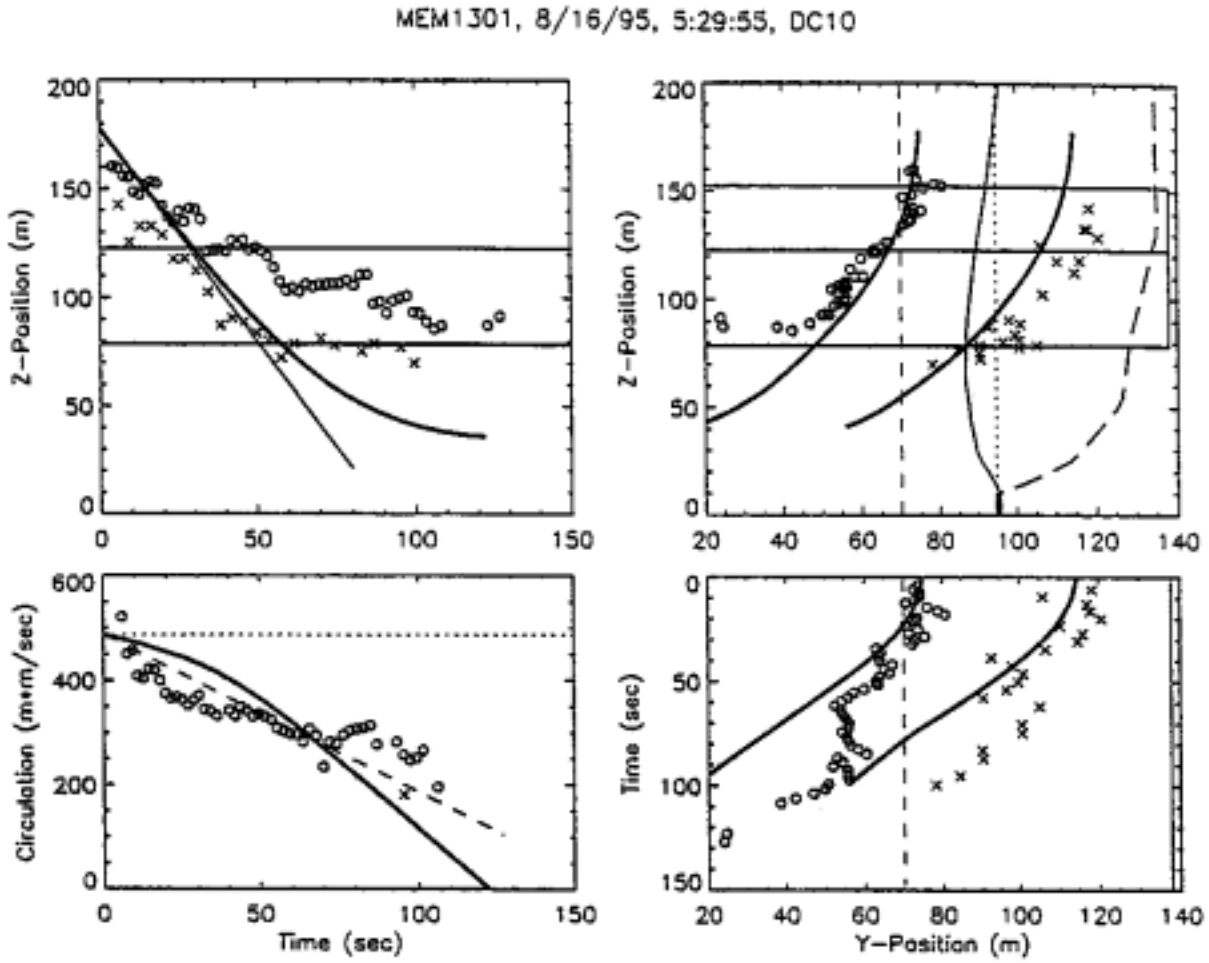


Figure B-1. EDR predictions versus observations for Case MEM 1301

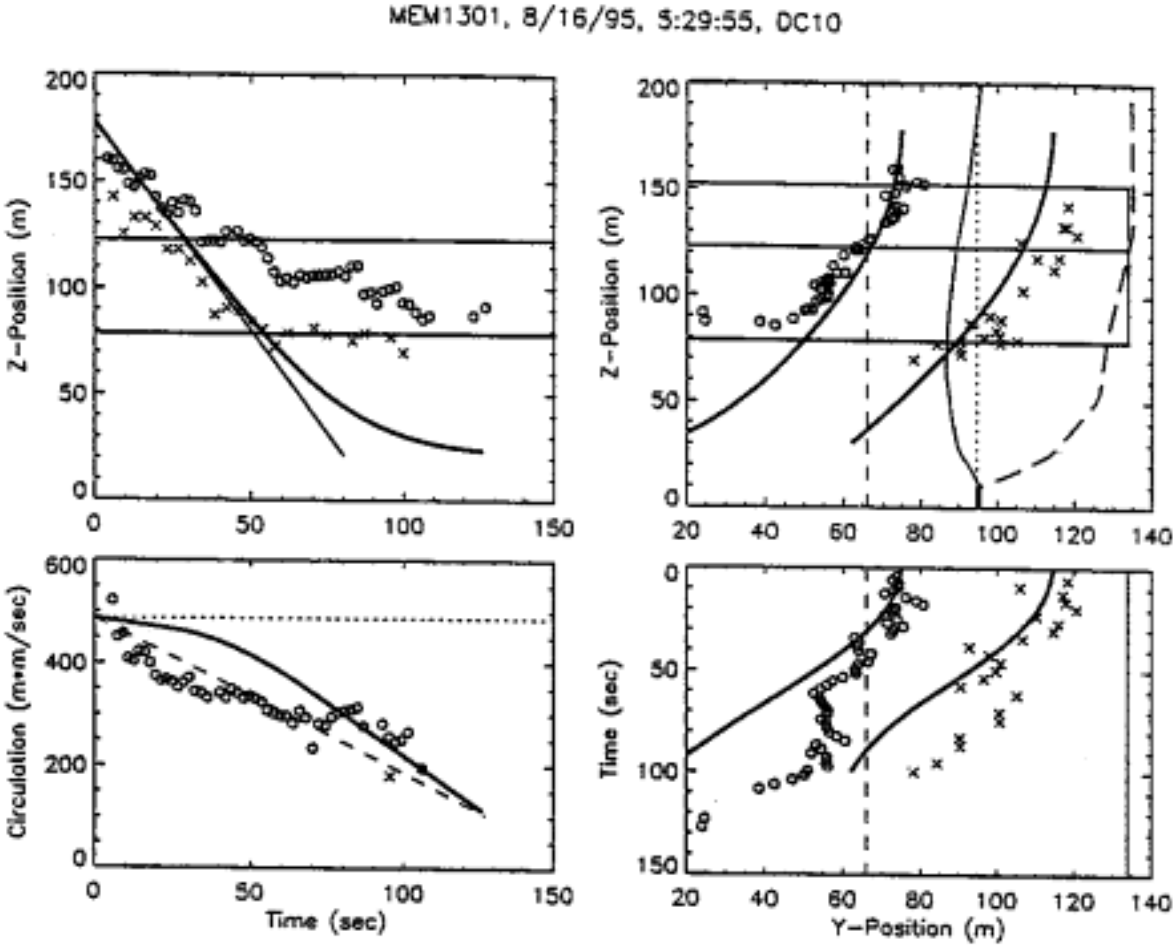


Figure B-2. TKE predictions versus observations for Case MEM 1301

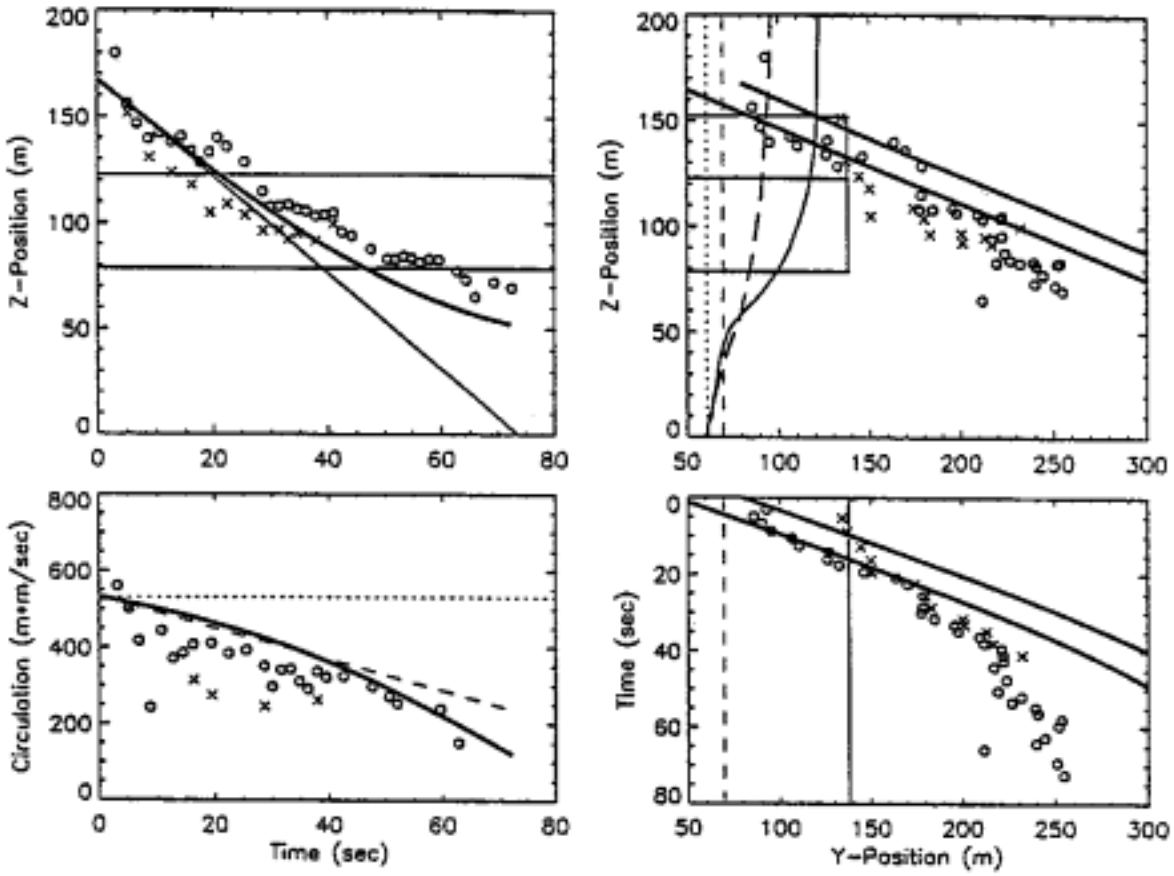


Figure B-3. EDR predictions versus observations for Case MEM 1245.

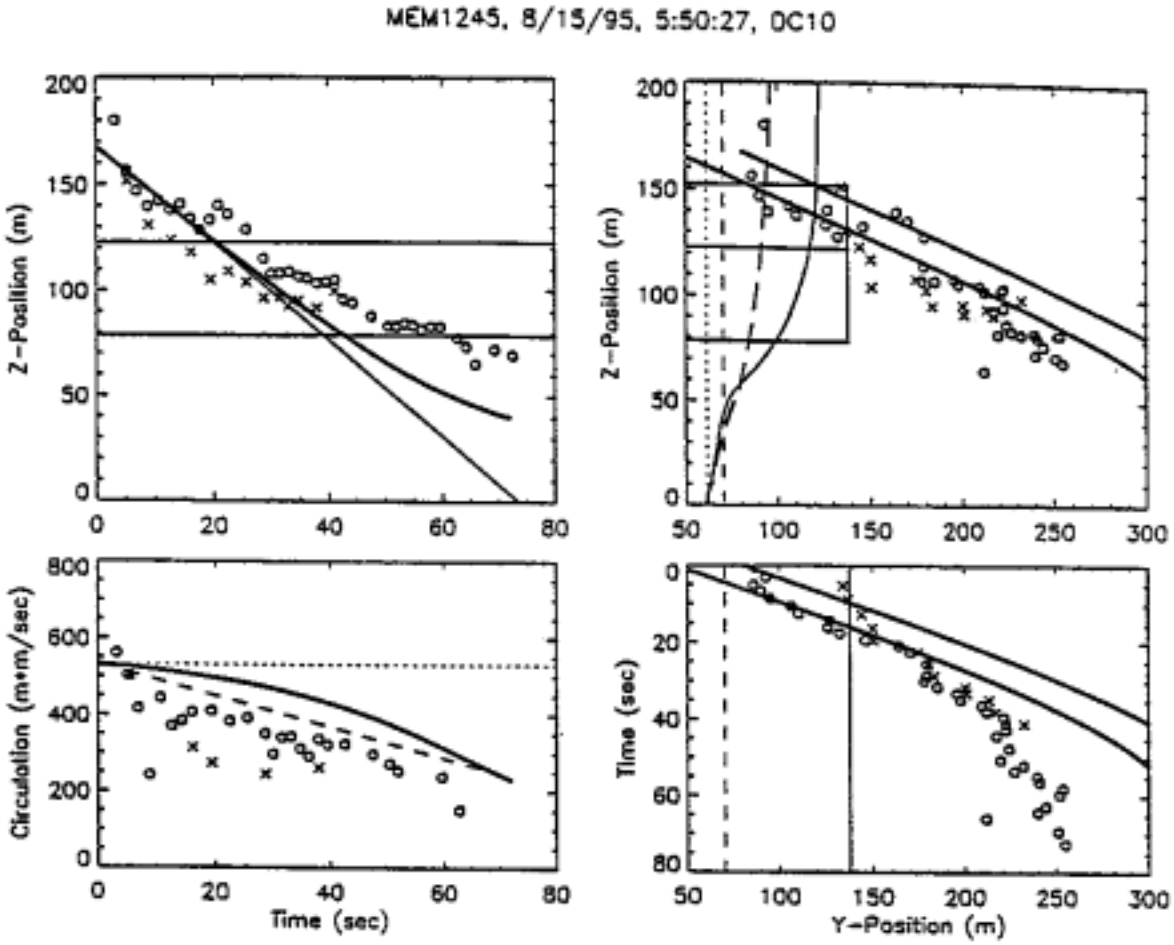


Figure B-4. TKE predictions versus observations for Case MEM 1245 .

## Appendix C. Supplementary Performance Statistics for EDR Model

In this appendix, we present a series of tables that provide statistical information which supplements the results presented in the main body of the report. We choose to examine results from only the EDR Model since it was seen to perform slightly better than the TKE Model, and it is the model currently being used by AVOSS.

Tables C.1-1 and C.1-2 show a breakdown of all cases used in scoring the models. The former table shows the number of cases from MEM and DFW that fall into various categories determined by observations and predictions of whether and how vortices leave the AVOSS corridor. The latter table shows the number of cases in various categories determined by observations and predictions of whether or not the circulation of vortices decays below 150 $m^2$/sec.

Additional statistics are given in subsequent tables for the first two categories in Table C.1-1 (vortices predicted and observed to leave the AVOSS corridor (1) through the floor and (2) through the side), and for the first category in Table C.1-2 (vortices' circulations predicted and observed to decay below 150 $m^2$/sec). Tables C.2-1, C.2-2, C.2-3 and C.2-4 examine the first two categories in Table C.1-1, and show how the errors between predictions and observations of corridor exit times are distributed with respect to ranges of observed exit times. Tables C.3-1 and C.3-2 examine the first category in Table C.1-2, and show how the errors between predictions and observations of the time for circulation to decay below 150 $m^2$/sec are distributed with respect to ranges of observed times for circulation to decay below 150 $m^2$/sec. Finally, Table C.4 shows how errors between predictions and observations for the cases included in Tables C.2-1, C.2-2, C.2-3 and C.2-4 and Tables C.3-1 and C.3-2 depend on atmospheric conditions.

Some observations on the data in the tables are as follows:

Tables C.1-1 and C.1-2 define which cases can be used for quantitative analysis of model predictions. Only the first two categories in Table C.1-1 and the first category in Table C.1-2 contain cases which allow quantitative comparison of predictions and observations. This is because times for exits through the side of the corridor cannot be meaningfully compared with exit times through the corridor floor, and finite times cannot be assigned to cases where vortices remain inside the corridor or circulation does not decay below a given threshold. Two categories in the tables are of operational interest to AVOSS. In Table C.1-1, there are 4 MEM and 7 DFW cases where vortices are predicted to leave the corridor, but observed to remain in the corridor, and in Table C.1-2, there are 46 MEM and 21 DFW cases where the circulation is predicted to decay below a given threshold but observed to remain above it. These cases are what might be called "false safe" cases, and in an operational AVOSS, actual observations would be required to alert Air Traffic Control to the possibility that suggested aircraft spacings based on such predictions might need to be reviewed.

Tables C.2-1 and C.2-2 contain results for the 140 exit-the-corridor-through-the-floor cases and the 21 exit-the-corridor-through-the-side cases from MEM. Table C.2-1 shows that the best predictions of time-to-leave-the-corridor-through-the-floor occur for vortices having observed vertical exit times in the range 15 to 25 seconds. In Table C.2-2, there is an insufficient number of cases to reach clear conclusions about predictions of time-to-leave-the-corridor-through-the-side, although the existing cases show results comparable with the best exit-through-the-floor results.

Tables C.2-3 and C.2-4 contain results for the 161 exit-the-corridor-through-the-floor cases and 5 exit-the-corridor-through-the-side cases from DFW. Table C.2-3 shows that the best predictions of time-to-leave-the-corridor-through-the-floor occur for vortices having observed vertical exit times in the range 10 to 25 seconds. In Table C.2-4, there is an insufficient number of cases to reach clear conclusions about predictions of time-to-leave-the-corridor-through-the-side, although the existing cases show results comparable with the best exit-through-the-side results.

Tables C.3-1 and C.3-2, respectively, contain results for the 111 circulation-decay-below-the-threshold cases from MEM and the 112 similar cases from DFW. Table C.3-1 shows that the best predictions of time-for-circulation-to-decay-below-the-threshold for vortices observed at MEM occur for the 60 cases where the observed time for circulation-to-decay-below-the-threshold is in the range 30-70 seconds. Table C.3-2 shows that the best predictions for vortices observed at DFW occur for the 57 cases where the range is 20-40 seconds. The difference in the best-prediction time ranges for MEM and DFW is probably due to the fact that most DFW cases occurred during the day whereas most MEM cases occurred in the late evening, and circulation decay rates are generally greater during the day than after sunset.

Table C.4 shows the effect of certain atmospheric conditions on the prediction-versus-observation errors for the cases included in Tables C.2-1, C.2-2, C.2-3 and C.2-4 and Tables C.3-1 and C.3-2. Atmospheric conditions considered are stratification, cross wind speed, and turbulence. These conditions are characterized by FRAV, VMAX* and EAVN, where FRAV is the average Froude number, VMAX* is the maximum cross-wind magnitude, and EAVN is the normalized average EDR; these quantities are evaluated by considering all data over the altitude range traversed by the vortices for each case.

If we first look at errors in prediction of time to leave the corridor through the floor (TTLCF), we see that the only atmospheric condition that has a notable effect for MEM and DFW cases is VMAX*, and this effect is not large. It appears that predictions of TTLCF are slightly better for high VMAX* than for low VMAX*, where the dividing line between high and low is a value of 1.6 m/sec (about 3 knots). At this time, we do not understand the underlying reason for this result, although an explanation may follow from the possibility that higher wind speeds may reduce effects of convection on vertical transport.

If we next consider the errors in prediction of time to leave the corridor through the side (TTLCS), we first observe that there are too few cases to reach any strong conclusions. However, it does appear, for MEM, that predictions are better for high stratification (low FRAV) and low turbulence (low EAVN), and that the low FRAV result is supported by the

small number of DFW cases. Here the dividing lines between high and low values of FRAV and EAVN, are the values 5 and 0.15, respectively. Since good predictions of TTLCS depend on having accurate cross wind profiles, a possible reason for the above result is that conditions of high stratification and low turbulence may promote high spatial correlation between the measured winds used in the model (derived from data taken on the order of a mile from the runway corridors) and the actual winds (which affect lateral transport of the vortices in the runway corridor). We also note that all TTLCS cases are associated with high VMAX*, which is what we would expect.

Finally, we examine errors in prediction of time for the vortices' circulation to drop below a given threshold (TFCTDBT), which for our purposes is 150 $m^2$/sec. We note that TFCTDBT predictions are better for low stratification (high FRAV) and high turbulence, for both MEM and DFW cases. A possible reason for this result is that the EDR model term for the effect of turbulence on circulation decay may be most accurate for low stratification and high turbulence.

**Table C.1-1: Statistics for Vortices Leaving Corridor**

| Behavior | Number of Cases MEM | DFW |
|---|---|---|
| Predicted and observed leave through floor | 140 | 161 |
| Predicted and observed leave through side | 21 | 5 |
| Predicted through floor, observed through side | 6 | 4 |
| Predicted through side, observed through floor | 20 | 10 |
| Predicted and observed remain | 1 | 1 |
| Predicted remain, observed leave | 0 | 1 |
| Predicted leave, observed remain* | 4 | 7 |
| Leave before observed | 19 | 2 |

**Table C.1-2: Statistics for Circulation Decay below Threshold**

| Behavior | Number of Cases MEM | DFW |
|---|---|---|
| Predicted drop below, observed drop below | 111 | 112 |
| Predicted drop below, observed remain above* | 46 | 21 |
| Predicted remain above, observed remain above | 31 | 27 |
| Predicted remain above, observed drop below | 23 | 31 |

---

In the above tables, the behaviors are abbreviated to conserve space. In Table C.1-1, the term "remain" means the corridor is not exited, and the term "leave" means the corridor is exited through either the floor or the side. In Table C.1-2, the circulation threshold is 150 $m^2$/sec. The term "drop below" means circulation becomes lower than this threshold, and the term "remain above" means circulation remains above it.

* These categories are significant for AVOSS, since they represent cases for which the prediction indicates a no-hazard condition, while the observation indicates a possible hazard.

**Table C.2-1: F_Error versus OUTM for MEM**

| OUTM Range | N | Median Error | Maximum Error |
|---|---|---|---|
| 10 - 15 | 11 | 3.08 | 12.00 |
| 15 - 16 | 22 | 1.70 | 8.29 |
| 16 - 18 | 20 | 1.77 | 4.27 |
| 18 - 20 | 34 | 0.92 | 4.82 |
| 20 - 22 | 23 | 1.46 | 6.06 |
| 22 - 25 | 10 | 3.89 | 7.82 |
| 25 - 30 | 7 | 8.46 | 9.66 |
| 30 - 36 | 8 | 15.53 | 18.32 |
| 40 - 46 | 4 | 22.39 | 25.80 |
| > 46 | 1 | ---- | 46.49 |

**Table C.2-2: S_Error versus OUTM for MEM**

| OUTM Range | N | Median Error | Maximum Error |
|---|---|---|---|
| 7 - 15 | 12 | 0.77 | 3.56 |
| 15 - 27 | 8 | 1.28 | 8.54 |
| > 27 | 1 | ---- | 9.13 |

---

In the above tables, F_Error is the absolute difference between the predicted and observed time for a vortex to exit the corridor through the corridor floor, and S_Error is the absolute difference between the predicted and observed time for a vortex to exit the corridor through the side of the corridor. OUTM is the observed time for a vortex to exit the corridor. All times are in seconds.

**Table C.2-3: F_Error versus OUTM for DFW**

| OUTM Range | N | Median Error | Maximum Error |
|---|---|---|---|
| < 10 | 1 | ---- | 5.21 |
| 10 - 14 | 8 | 2.16 | 9.36 |
| 14 - 15 | 20 | 1.28 | 4.30 |
| 15 - 16 | 31 | 1.82 | 4.22 |
| 16 - 17 | 19 | 2.05 | 3.98 |
| 17 - 18 | 30 | 1.39 | 2.80 |
| 18 - 20 | 24 | 0.86 | 3.47 |
| 20 - 25 | 16 | 2.46 | 7.87 |
| 25 - 37 | 10 | 9.84 | 17.51 |
| > 37 | 2 | 25.19 | 28.61 |

**Table C.2-4: S_Error versus OUTM for DFW**

| OUTM Range | N | Median Error | Maximum Error |
|---|---|---|---|
| 6 - 10 | 5 | 0.80 | 3.84 |

---

In the above tables, F_Error is the absolute difference between the predicted and observed time for a vortex to exit the corridor through the corridor floor, and S_Error is the absolute difference between the predicted and observed time for a vortex to exit the corridor through the side of the corridor. OUTM is the observed time for a vortex to exit the corridor. All times are in seconds.

**Table C.3-1: T_Error versus DTM1 for MEM**

| DTM1 Range | N | Median Error | Maximum Error |
|---|---|---|---|
| < 10 | 1 | ---- | 19.52 |
| 10 - 20 | 15 | 9.04 | 26.19 |
| 20 - 30 | 14 | 10.08 | 28.24 |
| 30 - 40 | 21 | 7.40 | 23.56 |
| 40 - 50 | 12 | 6.80 | 18.44 |
| 50 - 60 | 9 | 8.22 | 25.34 |
| 60 - 70 | 18 | 7.14 | 27.33 |
| 70 - 80 | 9 | 11.05 | 27.45 |
| 80 - 100 | 6 | 16.86 | 44.82 |
| > 100 | 6 | 39.45 | 58.98 |

**Table C.3-2: T_Error versus DTM1 for DFW**

| DTM1 Range | N | Median Error | Maximum Error |
|---|---|---|---|
| < 10 | 1 | ---- | 7.37 |
| 10 - 20 | 14 | 12.00 | 25.83 |
| 20 - 30 | 42 | 6.10 | 17.32 |
| 30 - 40 | 15 | 4.85 | 9.06 |
| 40 - 50 | 15 | 10.35 | 24.14 |
| 50 - 60 | 12 | 15.22 | 24.22 |
| 60 - 80 | 8 | 13.65 | 26.25 |
| 80 - 100 | 5 | 27.35 | 51.80 |

---

In the above tables, T_Error is the absolute difference between the predicted and observed time for a vortex's circulation to decay below the threshold of 150 $m^2$/sec. DTM1 is the observed time for a vortex's circulation to drop below this threshold. All times are in seconds.

**Table C.4: Atmospheric Effects on Model Performance Statistics**

| SITE | CONDITION | TTLCF Error | | | TTLCS Error | | | TFCTDBT Error | | |
|---|---|---|---|---|---|---|---|---|---|---|
| | | N | Mean | S.D. | N | Mean | S.D. | N | Mean | S.D. |
| MEM | | | | | | | | | | |
| | low FRAV | 82 | 4.279 | 6.878 | 11 | 0.653 | 0.358 | 49 | 13.984 | 12.487 |
| | high FRAV | 58 | 3.905 | 4.703 | 10 | 3.299 | 3.265 | 70 | 10.509 | 9.748 |
| | low VMAX* | 89 | 4.655 | 7.099 | 0 | ---- | ---- | 62 | 12.351 | 12.954 |
| | high VMAX* | 51 | 3.196 | 3.449 | 21 | 1.913 | 2.587 | 49 | 11.654 | 8.371 |
| | low EAVN | 121 | 4.118 | 6.305 | 18 | 1.604 | 2.138 | 92 | 12.807 | 11.664 |
| | high EAVN | 19 | 4.161 | 4.263 | 3 | 3.770 | 4.699 | 19 | 8.343 | 7.137 |
| | ALL | 140 | 4.124 | 6.056 | 21 | 1.913 | 2.587 | 111 | 12.043 | 11.124 |
| DFW | | | | | | | | | | |
| | low FRAV | 35 | 2.705 | 2.461 | 1 | 0.586 | ---- | 29 | 10.852 | 7.318 |
| | high FRAV | 126 | 2.693 | 3.936 | 4 | 1.428 | 1.645 | 83 | 9.832 | 8.852 |
| | low VMAX* | 84 | 3.101 | 4.453 | 0 | ---- | ---- | 55 | 9.793 | 8.837 |
| | high VMAX* | 77 | 2.253 | 2.481 | 5 | 1.259 | 1.473 | 57 | 10.389 | 8.151 |
| | low EAVN | 30 | 2.265 | 1.872 | 0 | ---- | ---- | 23 | 11.512 | 7.624 |
| | high EAVN | 131 | 2.794 | 3.955 | 5 | 1.259 | 1.473 | 89 | 9.730 | 8.667 |
| | ALL | 161 | 2.695 | 3.659 | 5 | 1.259 | 1.473 | 112 | 10.096 | 8.462 |

In the above table, TTLCF Error is the absolute difference between the predicted and observed time for a vortex to leave the corridor through the floor, TTLCS Error is the absolute difference between the predicted and observed time for a vortex to leave the corridor through the side, and TFCTDBT Error is the absolute difference between the predicted and observed time for a vortex's circulation to drop below the threshold 150 $m^2$/sec. All times are in seconds. The meaning of the CONDITIONS are as follows: the boundary between low FRAV and high FRAV is FRAV = 5, where FRAV is the average Froude number over the vortex altitude range; the boundary between low VMAX* and high VMAX* is 1.6 m/sec (about 3 knots), where VMAX* is the maximum cross-wind magnitude over the vortex altitude range; and the boundary between low EAVN and high EAVN is 0.15, where EAVN is the normalized average EDR over the vortex altitude range.

# REPORT DOCUMENTATION PAGE

*Form Approved*
*OMB No. 0704-0188*



| 1. AGENCY USE ONLY (*Leave blank*) | 2. REPORT DATE | 3. REPORT TYPE AND DATES COVERED |
|---|---|---|
| | June 2002 | Contractor Report |

**4. TITLE AND SUBTITLE**
Wake Vortex Algorithm Scoring Results

**5. FUNDING NUMBERS**
NAS1-99074

727-04-10-01

**6. AUTHOR(S)**
R. E. Robins and D. P. Delisi

**7. PERFORMING ORGANIZATION NAME(S) AND ADDRESS(ES)**
Northwest Research Associates, Inc.
14508 NE 20th Street
Bellevue, WA 98007-3713

**8. PERFORMING ORGANIZATION REPORT NUMBER**
NWRA-CR-00-R229B

**9. SPONSORING/MONITORING AGENCY NAME(S) AND ADDRESS(ES)**
National Aeronautics and Space Administration
Langley Research Center
Hampton, VA 23681-2199

**10. SPONSORING/MONITORING AGENCY REPORT NUMBER**
NASA/CR-2002-211745

**11. SUPPLEMENTARY NOTES**
Langley Technical Monitor: David Hinton

**12a. DISTRIBUTION/AVAILABILITY STATEMENT**
Unclassified-Unlimited
Subject Category 3 Distribution: Nonstandard
Availability: NASA CASI (301) 621-0390

**12b. DISTRIBUTION CODE**

**13. ABSTRACT** *(Maximum 200 words)*

This report compares the performance of two models of trailing vortex evolution for which interaction with the ground is not a significant factor. One model uses eddy dissipation rate (EDR) and the other uses the kinetic energy of turbulence fluctuations (TKE) to represent the effect of turbulence. In other respects, the models are nearly identical. The models are evaluated by comparing their predictions of circulation decay, vertical descent, and lateral transport to observations for over four hundred cases from Memphis and Dallas / Fort Worth International Airports. These observations were obtained during deployments in support of NASA's Aircraft Vortex Spacing System (AVOSS). The results of the comparisons show that the EDR model usually performs slightly better than the TKE model.

**14. SUBJECT TERMS**
aircraft approach spacing; aircraft wakes; wing tip vortices

**15. NUMBER OF PAGES**
44

**16. PRICE CODE**

| 17. SECURITY CLASSIFICATION OF REPORT | 18. SECURITY CLASSIFICATION OF THIS PAGE | 19. SECURITY CLASSIFICATION OF ABSTRACT | 20. LIMITATION OF ABSTRACT |
|---|---|---|---|
| Unclassified | Unclassified | Unclassified | UL |